Robotica (2022), **40**, pp. 4056–4075
doi:10.1017/S0263574722000753

CAMBRIDGE UNIVERSITY PRESS

RESEARCH ARTICLE

Design optimization of an underactuated tendon-driven anthropomorphic hand based on grasp quality measures

Hirakjyoti Basumatary* and Shyamanta M. Hazarika

Indian Institute of Technology, Guwahati, Biomimetic Robotics and Artificial Intelligence Laboratory (BRAIL), Mechanical Engineering Department, Guwahati, India, 781039
*Corresponding author. E-mail: b.hirak@iitg.ac.in

Received: 19 April 2021; **Accepted:** 8 May 2022; **First published online:** 21 June 2022

Keywords: Anthropomorphic underactuated hand, optimization, Potential grasp robustness, Grasp quality measure, Grasp wrench space

Abstract

For an underactuated anthropomorphic hand, apart from replicating the geometry, biomimicry of human counterpart requires design based on functional biomimesis. Optimization based on grasping capabilities to generate a stable grasp for underactuated anthropomorphic hands has been a recent focus. In this article, we optimize the actuation parameters of the underactuated mechanism based on grasp quality measures. Optimization of the hand design parameters like pulley radii, spring stiffnesses, and pre-load angles was undertaken based upon the grasp robustness metric. A quasi-static model based on a soft synergistic compliant grasp of the underactuated hand is formalized. Numerical simulations based on evolutionary strategies are applied to the grasp model to optimize the underactuated parameters. Finally, validation of the results based on the grasp wrench space is presented. The results show that an anthropomorphic hand with an optimized underactuated mechanism performs better grasps.

1. Introduction

The human hand is an intricate organ resulting from millions of years of evolution, helping us interact with the world around us. The loss of a hand can affect a person both physically and psychologically. This motivates numerous researchers to actively work on hand prostheses to improve and augment the life of amputees [1, 2]. The complexity of prostheses can vary from single to multidegree of freedom. See ref. [3] for an overview. Anthropomorphic robot hands help improve the embodiment of prosthetic hands. However, the cost (and possibly the weight) of a prosthetic device increases as the complexity and functionality increase [4]. One approach that could help bring down not only the weight but also the cost is by introducing underactuation. Underactuation usually means a mechanism with lower actuators than the total degrees of freedom (DoF) [5]. Consequently, the system cannot be commanded to follow arbitrary trajectories in configuration space. Nevertheless, the benefits of underactuation, such as lower weight and lower control requirements during grasping, outweigh the above restriction [6]. However, designing an efficient underactuated anthropomorphic prosthetic hand is a challenging task. The challenge comes from the perspective of building an underactuated mechanism maintaining the functional biomimesis.

Synergies of the hand usually refer to those variables that can demonstrate and recreate the intricate human hand movements and configurations, even if reduced in dimension compared to the hand DoF. Synergy-based control of an underactuated hand aids in accomplishing the different grasp types by helping control the synergies directly, rather than controlling individual DOFs. Implementing the synergies on an anthropomorphic robot hand can control the joints with fewer inputs [7]. Synergies could be exploited by multi-fingered underactuated anthropomorphic hands to perform a multitude of grasps. Here, the focus is on the five important grasp types of daily living activities, that is, power grasp (G_{pow}),

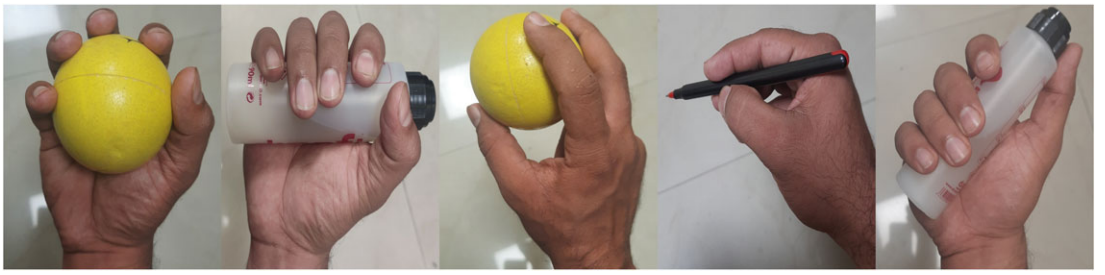

Figure 1. *Human hand grasp types: (a) Power grasp (b) Cylindrical grasp (c) Precision grasp (4) Pinch grasp (5) Oblique grasp.*

cylindrical grasp (G_{cyl}), precision grasp (G_{pre}), pinch grasp (G_{pin}), and oblique grasp (G_{obl}),(where G represents Grasp Matrix), as shown in Fig. 1. These grasps are considered as they are involved in more than 70% of the daily living activities [8]. Utilizing a synergy coupling matrix can help achieve underactuation and produce grasps with high quality, which aids in maintaining the functional biomimesis. Grasp quality is measured by the level of goodness of the grasp, which is determined by the properties like disturbance resistance, dexterity, equilibrium, and stability [9].

In this article, we optimize the actuation parameters based on grasp quality metrics and unbalanced torque methodologies. We consider a soft synergistic compliant grasping model and provide an optimization framework that aids in getting the optimal actuation parameters of an underactuated anthropomorphic hand based on the grasp robustness metric. We validate the proposed hand design through grasping experiments in a simulated environment and evaluate the grasp wrench space (GWS). The main contribution of this article is to propose a framework that aids in designing an anthropomorphic underactuated hand capable of generating grasps with sufficiently good quality.

The paper is organized as follows: The related work is discussed in Section 2. Section 3 provides a quick overview of the grasp quality metric-based optimization. Section 4 presents an overview of the problem formulation. The overall design methodology is reported in Section 5. The results of the numerical simulation and its validation are discussed in Section 6. Finally, we provide the conclusion of the work in Section 7.

2. Related work

While researchers have optimized the design of underactuated non-anthropomorphic grippers on many instances [10, 11, 12, 13, 14], this form of optimization is far less prevalent among anthropomorphic hands. Recently, there has been research on optimization of anthropomorphic hand-design for fully actuated hands based on a novel performance index for its kinematic properties referred to as "interactivity of fingers" [15]. There is also recent literature on kinematic optimization of underactuated hand based on maximizing the workspace intersection and maximizing the size of the largest graspable object [2]. However, it is concerned with kinematics rather than formulating the design based on grasping capabilities.

Optimization based on grasping capabilities is necessary to generate a stable grasp based on force closure properties and to enable disturbance handling. This is an area of active research to arrive at functional biomimesis. Recently, Chen et al. [16] performed design optimization based on the unbalanced torque method of the mechanically realizable manifold in posture and torque space by checking implementable grasp synergies. However, there remains the requirement of optimizing the design of the underactuated hand based on some grasp quality measures, as we are not aware of any reported in the literature. As discussed in the literature, there are many grasp quality measures [9]. However, few talk about grasp quality metrics for underactuated hands. Pozzi et al. [17] gave two measures of grasp quality for underactuated hand: (i) modified version of the largest-minimum resisted wrench to handle

https://doi.org/10.1017/S0263574722000753 Published online by Cambridge University Press

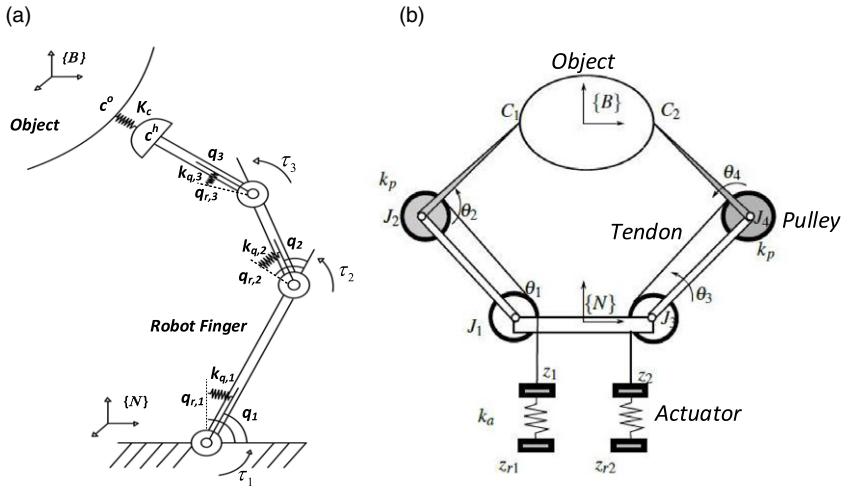

Figure 2. *Compliant Grasping (a) Compliant joints and compliant contacts with visualization of points, vectors and geometry, adapted from ref. [20] (b) Complaint underactuated hand with passive elastic elements in the joints J_2 and J_4, actuated by two elastic tendons, adapted from ref. [19].*

the underactuation; (ii) two robustness indices that can be used to measure grasp quality. One of the robustness indices is the contact robustness metric, known as potential contact robustness (PCR) and the other is grasp robustness metric called potential grasp robustness (PGR). Contact robustness is the ability of the contact to resist itself from violating contact constraints, whereas grasp robustness is the ability of the grasp to overcome the object immobilization constraint [18].

3. Grasp quality metric-based optimization for compliant anthropomorphic hands

3.1. The complaint grasp model

The mathematical model of grasping must represent the behavior of the hand and the grasped object while applying varied loading conditions. The most desirable quality while grasping is the capacity to maintain grasp stability in the face of unknown disturbance forces and moments applied to the object. The rigid body grasping model is the basic mathematical model of grasping. According to this model, in static equilibrium conditions, utilizing the principle of virtual work, we can write the equation of object and hand equilibrium, respectively, as [19]:

$$\boldsymbol{w} = -G\boldsymbol{\lambda} \tag{1}$$

$$\boldsymbol{\tau} = J^T\boldsymbol{\lambda} \tag{2}$$

However, extending the rigid body grasping model to include compliance is more realistic [20]. Analyzing a grasp through the complaint grasping model increases the dexterous manipulability and robustness of static grasps as it helps implement desired compliance behaviors while grasping an object. In modeling the compliant grasp, a set of hypothetical springs are introduced at the contact locations between the object and the fingers. Figure 2(a) shows the complaint joints, complaint contacts, and the different vectors like joint variables $\boldsymbol{q}$, $\boldsymbol{q}_r$, $\boldsymbol{\tau}$, etc. In modeling the compliant grasp, a set of hypothetical springs are introduced at the contact locations between the object and the fingers. The contact force variation $\delta\boldsymbol{\lambda}$ from the initial equilibrium position is given as

$$\delta\boldsymbol{\lambda} = K_c(\delta\boldsymbol{c}^h - \delta\boldsymbol{c}^o) = K_c(J\delta\boldsymbol{q} - G^T\delta\boldsymbol{u}) \tag{3}$$

https://doi.org/10.1017/S0263574722000753 Published online by Cambridge University Press

Table I. *Nomenclature.*

Notation	Definition
$\boldsymbol{w} \in \mathbb{R}^6$	External wrench
$\boldsymbol{\tau} \in \mathbb{R}^{n_q}$	Joint torque
n_q	Number of hand joints
n_c	Number of contact points
$n_\lambda = 3n_c$	Single point contact with friction
$\boldsymbol{\lambda} \in \mathbb{R}^{n_\lambda}$	Generic contact forces
$G \in \mathbb{R}^{6\times n_\lambda}$	Grasp matrix
$J \in \mathbb{R}^{n_\lambda \times n_q}$	Hand jacobian
K_c	Contact stiffness matrix
$\boldsymbol{c^h}$	Contact location on the hand
$\boldsymbol{c^o}$	Contact location on the object
$\delta \boldsymbol{x}$	Change in $\boldsymbol{x}$; where $\boldsymbol{x}$ is a variable
$\boldsymbol{q} \in \mathbb{R}^{n_q}$	Joint displacement
$\boldsymbol{u}$	Object position
K_q	Joint stiffness matrix
S	Synergy matrix
S_a	Synergy matrix of active tendons
S_p	Synergy matrix of passive tendons
$\boldsymbol{\sigma}$	Langragian co-ordinate contact forces
K_{za}	Active joint stiffness
$\boldsymbol{z_a}$	Actual actuator position
$\boldsymbol{z_p}$	Passive input position
$\boldsymbol{z_{ra}}$	Reference actuator position
K_{zp}	Passive joint stiffness
K_z	Synergy stiffness
$\boldsymbol{z_r}$	Synergy reference value
μ_i	Friction coefficient of i^{th} contact
$\boldsymbol{\lambda_{i,n}}$	Normal contact force i^{th} contact
$\boldsymbol{\lambda_{i,t}}$ and $\boldsymbol{\lambda_{i,o}}$	Tangential contact force i^{th} contact

The actual joint variables, $\boldsymbol{q}$, may differ from the reference one, $\boldsymbol{q_r}$, if the hand structural parameters are not perfectly stiff. This can be modeled as

$$\delta \boldsymbol{\tau} = K_q(\delta \boldsymbol{q_r} - \delta \boldsymbol{q}) \tag{4}$$

Further to include the concept of underactuation, the concept of postural synergies from neuroscience can be utilized. According to postural synergies, the most commonly seen postures in human hand movement can be defined by a reduced dimension of principal directions in hand configuration space. The postural synergy model, on the other hand, is good for creating pre-shaping grasp phases but not for predicting how grasping forces are formed after contact. As a result, a soft synergistic model with compliance is used to account for forces emerging from resistance to interpenetration of bodies. This model allows a feasible grasping model for an underactuated robotic hand. Figure 2(b) shows an example of compliant underactuated hand grasping an object. In this figure, the 4 DOFs hand is actuated by two actuators through a tendon-pulley transmission mechanism and has passive elastic elements (springs) at two joints J_2 and J_4.

Considering the linear approximation of all the possible displacements around an equilibrium configuration while grasping an object and the synergistic underactuation, fundamental grasp equation (FGE) can be summarized, which takes into account all the above conditions [21]. For further details of the

https://doi.org/10.1017/S0263574722000753 Published online by Cambridge University Press

derivation of FGE, refer to Appendix A.

$$A\delta \boldsymbol{x} = \delta \boldsymbol{y} \tag{5}$$

$$A = \begin{bmatrix} -G & 0 & 0 & 0 & 0 & 0 & 0 \\ J^T & K_{J,u} & -I & K_{J,q} & 0 & 0 & 0 \\ 0 & 0 & S^T & 0 & -I & K_{S,z} & 0 \\ C_c & G^T & 0 & -J & 0 & 0 & 0 \\ 0 & 0 & -I & -K_q & 0 & 0 & K_q \\ 0 & 0 & 0 & 0 & C_z & I & 0 \\ 0 & 0 & 0 & 0 & 0 & S & -I \end{bmatrix} \tag{6}$$

$$\delta \boldsymbol{x} = \begin{bmatrix} \delta \boldsymbol{\lambda} & \delta \boldsymbol{u} & \delta \boldsymbol{\tau} & \delta \boldsymbol{q} & \delta \boldsymbol{\sigma} & \delta z & \delta \boldsymbol{q}_r \end{bmatrix}^T \tag{7}$$

$$\delta \boldsymbol{y} = [\delta \boldsymbol{w} \;\; 0 \;\; 0 \;\; 0 \;\; 0 \;\; \delta \boldsymbol{z}_r \;\; 0]^T \tag{8}$$

The linear system given by Eq. (5) can be solved to find $\delta \boldsymbol{x}$, if the square matrix A is not singular. Usually, matrix A is typically invertible. Conditions of its non-invertibility arises only when: condition (1) indeterminacy of the grasp, that is, nullspace of the transpose of grasp matrix ($\mathcal{N}(G^T)$) is non-trivial, condition (2) defectiveness of the grasp, that is, nullspace of the transpose of hand jacobian ($\mathcal{N}(J^T)$) is non-trivial. The above conditions arise when the total contacts are too limited, and the object displacement is not fully constrained by the contacts arising between the hand and the environment. Given $\delta \boldsymbol{z}_r$ and/or for a given $\delta \boldsymbol{w}$, a unique solution exists for Eq. (5), if the matrix, A is not singular. If we assume $\delta \boldsymbol{w} = 0, \delta \boldsymbol{z}_r \neq 0$ and solve, then it means for a given grasping system, what are the permissible controllable forces and motions acting on the hand and arm reference configuration. Further, the solution for the assumption $\delta \boldsymbol{w} \neq 0, \delta \boldsymbol{z}_r = 0$ demonstrates how much amount of external disturbances the robotic hand can withstand. External disturbances are represented as changes in the wrenches applied to the grasped object [22].

3.2. Grasp quality metric: Grasp robustness and contact robustness

Considering i-th contact, the contact forces $\boldsymbol{\lambda}_i$ requires to satisfy unilateral force constraint and Coulomb friction constraint. Eqs. (9) and (10) specifies the above conditions, respectively. These constraints helps in avoiding detachment and slip of the contact during object grasps.

$$\boldsymbol{\lambda}_{i,n} \geq 0 \tag{9}$$

$$\sqrt{\boldsymbol{\lambda}_{i,t}^2 + \boldsymbol{\lambda}_{i,o}^2} \leq \mu_i \boldsymbol{\lambda}_{i,n} \tag{10}$$

Given an object and a hand, there are usually many grasps that satisfy a desired grasp property. The quality of a good grasp is determined by its ability to take into account disturbance resistance, dexterity, equilibrium, and stability. As a result, to choose the optimal grasp, a quality measure, or an index that quantifies the goodness of a grasp, is used. This metric is commonly referred to as grasp quality measure in the literature [9]. There are other measures for grasp quality like PCR and PGR, which help in evaluating the contact robustness and grasp robustness, respectively. Contact robustness refers to the distances or how far a contact is from the violation of any contact constraint, whereas grasp robustness concerns how far the grasp is from overcoming the object immobilization constraint, that is, the ability to resist external disturbances. Details regarding PCR and PGR is included in Appendix B. PGR metric is considered better than the PCR metric because it considers the fact that even if some contact constraints are not satisfied, a hand can perform a stable grasp, whereas PCR is a conservative measure as it states that only if contact forces are applied at all the contact points, the grasp is stable

https://doi.org/10.1017/S0263574722000753 Published online by Cambridge University Press

Table II. *Co-efficients of constraints.*

Constraint type	$\eta_{i,k}$	$\gamma_{i,k}$	$\delta_{i,k}$
Friction cone($k=f$)	η_i	-1	0
Minimum normal force ($k=m$)	0	-1	f_i, min
Maximum force module($k=M$)	1	0	$-f_i, max$

[23, 18]. An improved method of evaluating PGR is discussed in the literature [24], which requires to analytically solve a problem that involves minimizing the cost function $V(y)$ described in the next section. This cost function is determined by contact properties such as contact surface geometry and friction coefficient, as well as contact forces. Based upon this, we have framed our objective function, which is discussed in the next section.

3.3. Objective function

The constraints of contact forces that needs to be satisfied while grasping, as defined in Eqs. (9) and (10), can be expressed as $\boldsymbol{\sigma_{i,t}} = \eta_i \|\boldsymbol{\lambda_i}\| - \boldsymbol{\lambda_{i,n}} < 0$ where $\eta_i = \left(\sqrt{1+\mu_i^2}\right)^{-1}$. Also, if we impose bounds on the contact force magnitude, then we can introduce two more constraints: (1) $\boldsymbol{\sigma_{i,m}} = \boldsymbol{f_{i,\min}} - \boldsymbol{\lambda_{i,n}} < 0$ (2) $\boldsymbol{\sigma_{i,M}} = \|\boldsymbol{\lambda_i}\| - \boldsymbol{f_{i,\max}} < 0$, where $f_{i,\min}$: lower bound and $\boldsymbol{f_{i,\max}}$: upper bound on the contact forces. Expressing the above constraints into a single inequality equation gives

$$\boldsymbol{\sigma_{i,k}} = \eta_{i,k} \|\boldsymbol{\lambda_i}\| + \gamma_{i,k}\boldsymbol{\lambda_{i,n}} + \delta_{i,k} < 0 \tag{11}$$

where, $i = 1, \ldots, n_c$: no. of contacts; k(constraint type) $= f, m, M$ and $\eta_{i,k}, \gamma_{i,k}$, *and* $\delta_{i,k}$ represents constant parameters defined in Table II.

A term $\Omega^{\in}_{i,k} \subset \mathbb{R}^h$ representing the set $\boldsymbol{y}$ for a given external wrench $\boldsymbol{w}$ is defined, satisfying the constraint in Eq. (11) by a margin $\in : \Omega^{\in}_{i,k} = \{\boldsymbol{y} | \boldsymbol{\sigma}_{i,k}(g, y) < -\in\}$

For each contact, i and constraint, k the below function can be defined:

$$V^{\in}_{i,k}(\mathbf{w}, \mathbf{y}) = \begin{Bmatrix} (d\boldsymbol{\sigma}^2_{i,k})^{-1} & \boldsymbol{y} \in \Omega^{\in}_{i,k} \\ a\boldsymbol{\sigma}^2_{i,k} + b\boldsymbol{\sigma}_{i,k} + c & \mathbf{y} \notin \Omega^{\in}_{i,k} \end{Bmatrix} \tag{12}$$

Friction constraints and contact force magnitude limitations are taken into account in the above cost function. The objective function for the grasp quality metric based optimization based on the above cost function can be defined as

$$V(\boldsymbol{w}, \boldsymbol{y}) = \sum_{i=1}^{n_c} \sum_{k=f,m,M} V^{\in}_{i,k}(\boldsymbol{w}, \boldsymbol{y}) \tag{13}$$

Then,

$$PCR = \frac{1}{V(\hat{\boldsymbol{y}})} \tag{14}$$

and,

$$PGR = \max_{C_j} \frac{1}{V(\hat{\boldsymbol{y}}, C_j)} = \max_{C_j} PCR(C_j) \tag{15}$$

$$subject \;\; to \quad \mathcal{N}(K(C_j)G^T) = 0 \tag{16}$$

4. Problem formulation

The goal is to optimize the underactuated parameters for the five grasps generated through synergies. We aim to achieve it through the optimization of grasp quality measures of the grasps. Hand kinematics of

https://doi.org/10.1017/S0263574722000753 Published online by Cambridge University Press

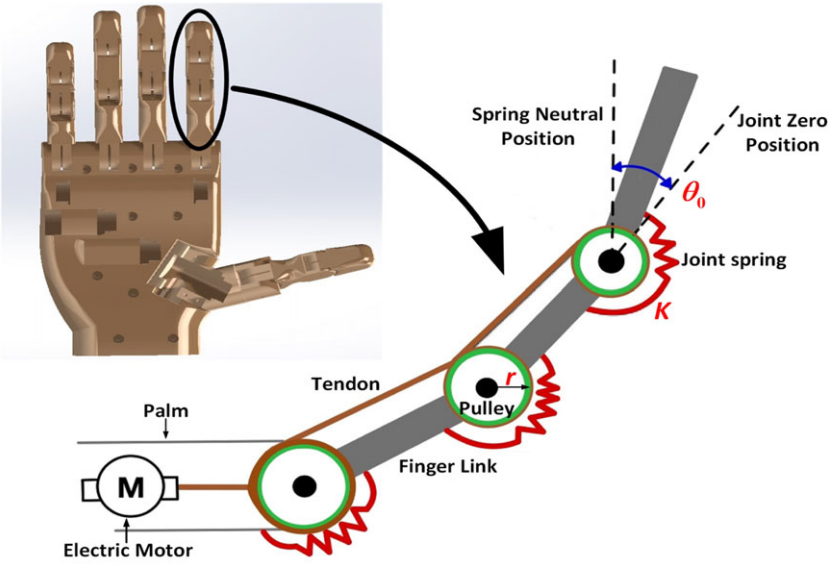

Figure 3. *Schematic of an underactuated finger. Design parameters to be optimized are shown in red, that is, r, K and θ_0.*

under-actuated hands usually include the specification of number, shape, size of fingers, tendon routing mechanism, size of the tendon moment arms, etc. The design space (all the possible design solutions) of the anthropomorphic hand was narrowed down by considering a hand with pre-defined kinematics and structure. We consider the kinematics where the tendons are routed around the pulleys. The flexion is achieved under the action of the tendon-driven mechanism, and the springs help in the extension of the fingers. The actuation parameters of the design space we choose to optimize includes (i) the pulley radius (i.e., the tendon moment arms of the joints): which helps in the efficient transmission of forces; (ii) the spring stiffness (passive actuators at the joints): which helps in extension and maintaining joint-stiffness; and, (iii) the spring pre-load angles: which helps maintain a feasible posture for grasp preshape before attempting different grasp types. The schematic of the underactuated finger and the design parameters to be optimized are shown in Fig. 3. The optimized parameters produce the most robust grasps for all the grasp postures.

5. Design methodology

5.1. Problem decomposition

The problem is a multi-objective optimization within the identified design space. Since, it is a high-dimensional optimization problem, it is not feasible to search for all the design variables simultaneously. Hence, we solve the optimization problem by decomposing it into a two-step process:

1. Optimization of the contact force distribution based on grasp quality
2. Optimization of the kinematic behavior based on unbalanced torque method

The motive for the decomposition is to mainly split the optimization problem for both the pre-contact and post-contact behavior. The post-contact contact force distribution based on the grasp quality to optimize the moment arms and spring stiffness is undertaken in the first step. Secondly, for the pre-contact kinematic behavior, we take into account the optimization of the spring pre-load angles for optimal grasp preshaping. The details of the two-step optimization is referred to in the next section.

https://doi.org/10.1017/S0263574722000753 Published online by Cambridge University Press

Algorithm 1: *Optimization of the tendon moment arms and spring stiffness.*

Initializing population of random candidates
for each combination of r and K **do**
  for $k \in \{G_{pow}, G_{pre}, G_{cyl}, G_{obl}, G_{pin}\}$ **do**
    Calculate PGR_k
  end for
  Calculate the co-efficient of variation of the PGRs, PGR_{cov}
end for
Select the combination of r and K that gives the minimum of all the PGR_{cov}s obtained, i.e., $r_{opt}, K_{opt} = min(PGR_{cov})$

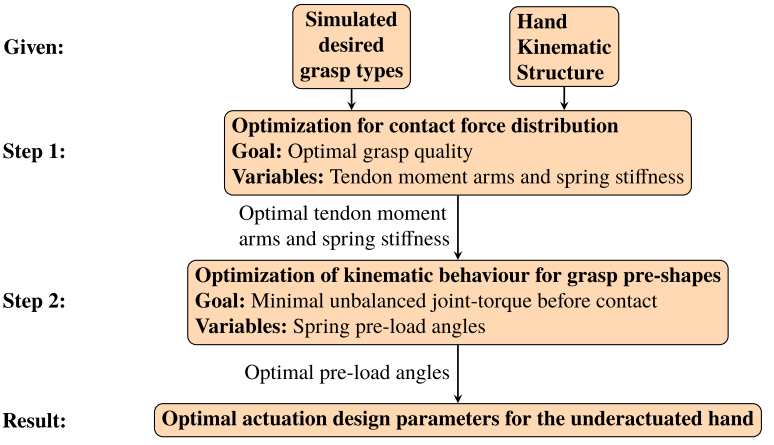

Figure 4. *Flowchart of the optimization.*

5.2. Optimization methodology

The flow chart of the proposed optimization framework is shown in Fig. 4. The optimization starts with pre-specified desired grasps and hand kinematics. First, in Step 1, we solve the optimal contact force distribution post-contact in the optimization framework as detailed in Algorithm 1. We then solve for the optimal parameters that contribute to the kinematic behaviors for grasp pre-shapes in Step 2, explained in detail in Algorithms 2 and 3. Finally, we get the optimal actuation parameters for the underactuated mechanism for both contact force distribution and posture shaping based on grasp quality measures. The evolutionary optimization algorithm utilized for obtaining the optimal parameters was the simulated annealing method. It is a meta-heuristic optimizer for global optimization in a large search space of an optimization problem. Normal heuristic optimizer like gradient ascent finds better neighbor solutions than current values and stop on reaching an optimal value that does not have neighbors with better solutions. Thus, arriving at it may be local optima, but a better solution may be located on other locations, which may be a global optimum that could be different from the current one. Meta-heuristics utilizes the nearby solutions to explore the search space, and while they too search for better neighboring solutions like the simple heuristics, yet they accept inferior neighbors to avoid getting stuck in local optima. Hence, they are able to find candidates of global optima in the stipulated time.

5.2.1. Optimization based on contact force distribution (after contact)

For optimizing the parameters based on contact force distribution after contact, we used grasp robustness as an evaluation property of the generated grasp. Given the grasp space, we perform the following optimization given in Algorithm 1.

The algorithm is an optimum global search over different tendon pulley radii (tendon moment arms) and spring stiffnesses for the five grasps, which are considered. We calculate the PGR metric for all five grasps. The objective function for the optimization framework is to minimize the overall coefficient of

https://doi.org/10.1017/S0263574722000753 Published online by Cambridge University Press

Algorithm 2: *Calculation of spring pre-load angles*

0: Initialize population of random candidates
1: **for** each combination of (θ_0) **do**
2: **for** each grasp type, i **do**
3: Compute $q_i = \|\delta\boldsymbol{\tau_b}\|$ using Algorithm 3
4: **end for**
5: Compute the overall stability metric $Q = \|[q_1, q_2, ...]\|$
6: **end for**
7: Output: θ_{0opt}, i.e., optimal $\theta_0 s$

Algorithm 3: *Calculation of stability metric pre-contact*

1. find: tendon tensions $(\boldsymbol{t})$
2. minimize: $\|\delta\boldsymbol{\tau_b}\|^2 = \boldsymbol{t}^T R^T R\boldsymbol{t} - 2\boldsymbol{\tau_s^T} R\boldsymbol{t} + \boldsymbol{\tau_s^2}$
3. subject to: taut tendons, i.e., $\boldsymbol{t} \geq 0$

variation (CV), also known as relative standard deviation (RSD), of the PGRs of the five grasps taken together, PGR_{cov}. Minimizing the CV or RSD proves to be beneficial as it aids in maximizing the PGR values to be located near the mean of the PGRs of all the grasps so that outliers have a lesser effect on the overall average metric.

5.2.2. Optimization based on unbalanced torque (before contact)

For the calculation of the spring pre-load angles, we used the same method of optimization, that is, unbalanced joint torque method before contact, as described in ref. [16]. In an underactuated mechanism, where a tendon connects different joints together, the norm of the unbalanced joint torques (before contact) is given as

$$\delta\boldsymbol{\tau_b} = R(r_1, r_2, \ldots.)\boldsymbol{t} - \boldsymbol{\tau}_s \tag{17}$$

where, t: unknown tendon tension vector, R: function of $r_1, r_2, \ldots$ (the optimized tendon moment arms from Algorithm 1), $\boldsymbol{\tau}_s = [K_1(\theta_1 + \theta_{01}), K_2(\theta_2 + \theta_{02}) \ldots]^T$: spring torques calculated by spring parameters and hand poses. The goal is to find $\boldsymbol{t}$ which would give the least norm of unbalanced joint torque before contact.

To search for the optimal pre-load angles, a two-layer framework is utilized. The outer layer performs an exhaustive search over the pre-load angles. The inner layer, which is a non-convex problem, computes the norm of unbalanced joint torques. The pseudo-code of the optimization framework is shown in Algorithms 2 and 3.

6. Design example and experimentation

A CAD model of the anthropomorphic hand was made in solidworks (see Fig. 5(a)). The measurement of the joint limits and material properties, that is, polylactic acid (PLA plastic), have been added to the assembly. Then, a replica of the hand model has been prepared on MATLAB for further analysis as shown in Fig. 5(b).

At first, we built different objects and actuated the joints to generate different grasps, as shown in Fig. 6. Then, we utilized the synergy coupling matrix given in Eq. (18), to replicate the coupling between the joints of the under-actuated anthropomorphic hand. The synergy coupling matrix is constant and is inspired by the example of the underactuated mechanism in ref. [25].

https://doi.org/10.1017/S0263574722000753 Published online by Cambridge University Press

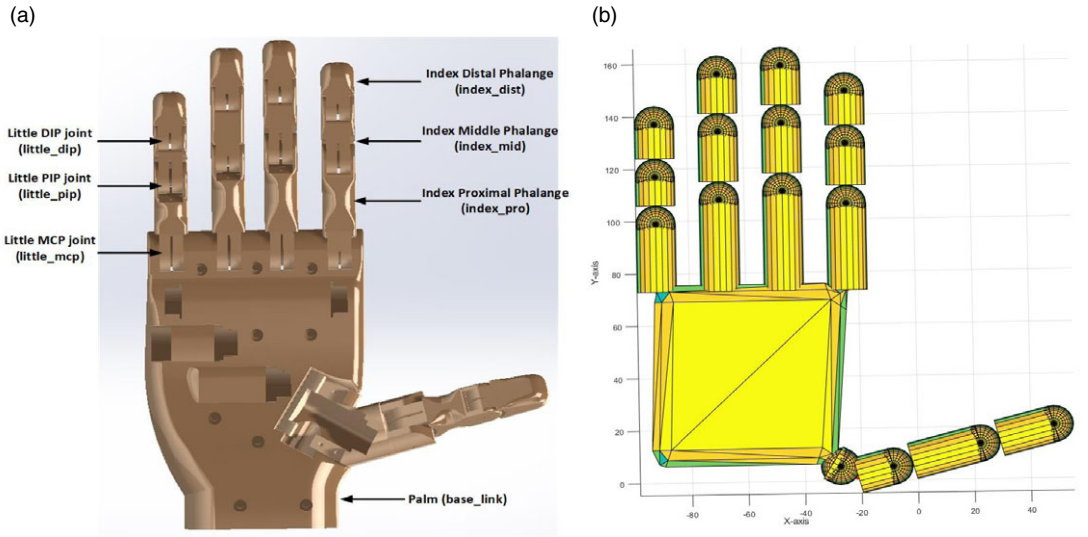

Figure 5. *Hand model (a) Solidworks CAD model (b) MATLAB Kinematic model.*

$$S = \begin{bmatrix}
1 & 0 & 0 & 0 & 0 & 0 & 0 & 0 & 0 & 0 & 0 & 0 & 0 & 0 & 0 & 0 \\
0 & \frac{1}{r1(t)} & -\frac{r2(t)}{r1(t)} & -\frac{r3(t)}{r2(t)} & 0 & 0 & 0 & 0 & 0 & 0 & 0 & 0 & 0 & 0 & 0 & 0 \\
0 & 0 & 1 & 0 & 0 & 0 & 0 & 0 & 0 & 0 & 0 & 0 & 0 & 0 & 0 & 0 \\
0 & 0 & 0 & 1 & 0 & 0 & 0 & 0 & 0 & 0 & 0 & 0 & 0 & 0 & 0 & 0 \\
0 & 0 & 0 & 0 & \frac{1}{r1(i)} & -\frac{r2(i)}{r1(i)} & -\frac{r3(i)}{r2(i)} & 0 & 0 & 0 & 0 & 0 & 0 & 0 & 0 & 0 \\
0 & 0 & 0 & 0 & 0 & 1 & 0 & 0 & 0 & 0 & 0 & 0 & 0 & 0 & 0 & 0 \\
0 & 0 & 0 & 0 & 0 & 0 & 1 & 0 & 0 & 0 & 0 & 0 & 0 & 0 & 0 & 0 \\
0 & 0 & 0 & 0 & 0 & 0 & 0 & \frac{1}{r1(m)} & -\frac{r2(m)}{r1(m)} & -\frac{r3(m)}{r2(m)} & 0 & 0 & 0 & 0 & 0 & 0 \\
0 & 0 & 0 & 0 & 0 & 0 & 0 & 0 & 1 & 0 & 0 & 0 & 0 & 0 & 0 & 0 \\
0 & 0 & 0 & 0 & 0 & 0 & 0 & 0 & 0 & 1 & 0 & 0 & 0 & 0 & 0 & 0 \\
0 & 0 & 0 & 0 & 0 & 0 & 0 & 0 & 0 & 0 & \frac{1}{r1(r)} & -\frac{r2(r)}{r1(r)} & -\frac{r3(r)}{r2(r)} & 0 & 0 & 0 \\
0 & 0 & 0 & 0 & 0 & 0 & 0 & 0 & 0 & 0 & 0 & 1 & 0 & 0 & 0 & 0 \\
0 & 0 & 0 & 0 & 0 & 0 & 0 & 0 & 0 & 0 & 0 & 0 & 1 & 0 & 0 & 0 \\
0 & 0 & 0 & 0 & 0 & 0 & 0 & 0 & 0 & 0 & 0 & 0 & 0 & \frac{1}{r1(l)} & -\frac{r2(l)}{r1(l)} & -\frac{r3(l)}{r2(l)} \\
0 & 0 & 0 & 0 & 0 & 0 & 0 & 0 & 0 & 0 & 0 & 0 & 0 & 0 & 1 & 0 \\
0 & 0 & 0 & 0 & 0 & 0 & 0 & 0 & 0 & 0 & 0 & 0 & 0 & 0 & 0 & 1
\end{bmatrix} \tag{18}$$

where $r1$, $r2$, and $r3$ are the pulley radii of the proximal, middle, and distal joints, respectively, and t, i, m, r, and l represents thumb, index, middle, ring, and little fingers, respectively.

6.1. Numerical simulations

The results were calculated using both the methods of optimization: grasp quality metric-based methodology and unbalanced torque optimization [16]. The later was done to compare and validate the results obtained through both the different methodologies. The upper and lower bound of the pulley sizes depended on the anthropomorphic hand design, whereas the bounds of spring stiffness depended on

https://doi.org/10.1017/S0263574722000753 Published online by Cambridge University Press

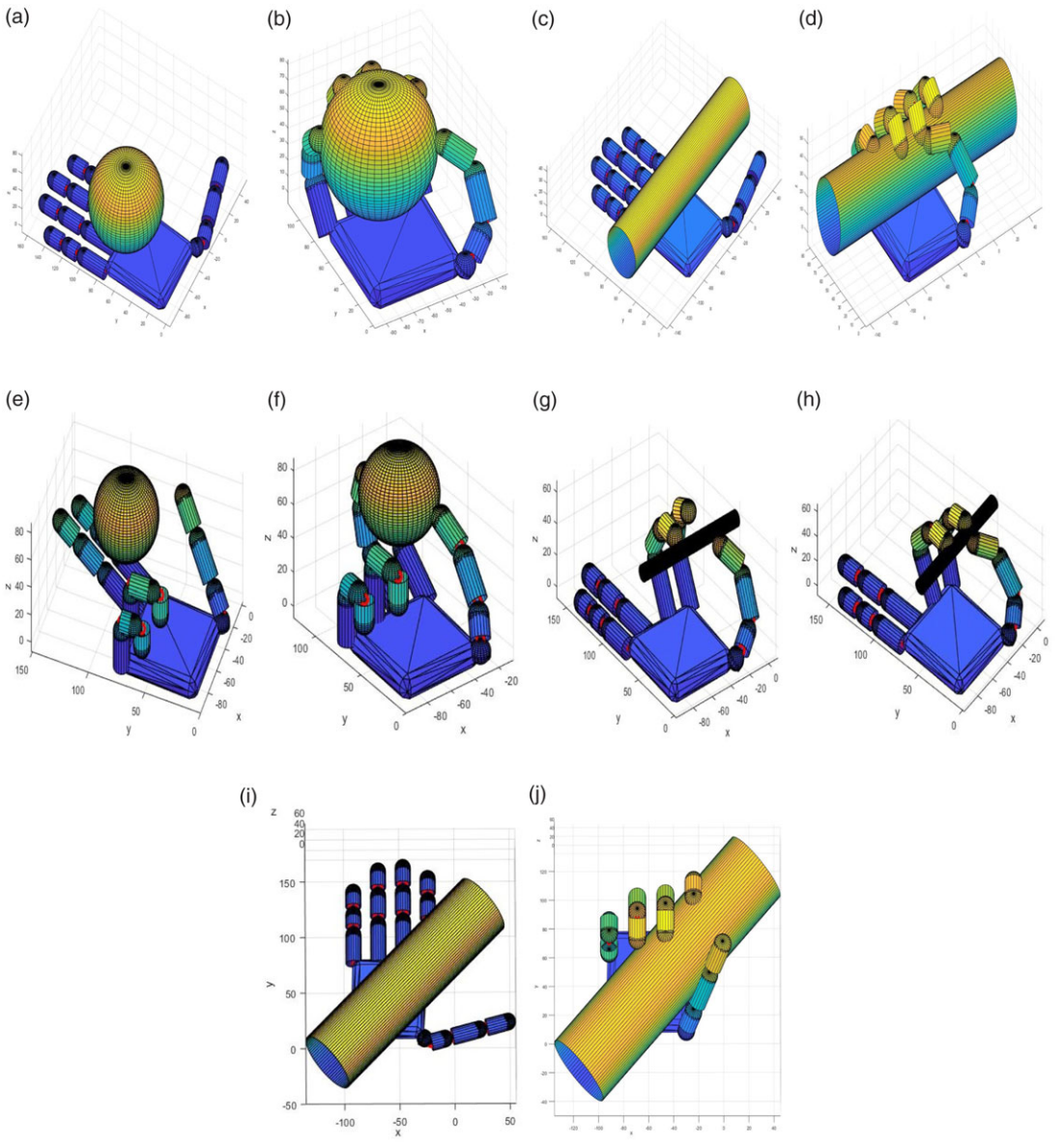

Figure 6. *Grasps generated in MATLAB (a) Power (initial) (b) Power (final) (c) Cylindrical (initial) (d) Cylindrical (final) (e) Precision (initial) (f) Precision (final) (g) Pinch (initial) (h) Pinch (final) (i) Oblique (initial) (j) Oblique (final).*

the mounting area and the allowed extension. The bounds on the pulley sizes were kept between 5 and 9 mm, and that of spring stiffness were kept as 0.05 to 0.10 N/mm. Further, the spring pre-load angles are bounded with respect to the maximum allowed torsional angle for the ability to attain different grasp shapes and generate enough restoring torque. The results of the optimization of pulley radius and spring pre-load angles through grasp quality methodology are shown in Table III and that of unbalanced torque are shown in Table IV. The spring stiffness obtained through the former and later optimization methodologies were 0.10 and 0.05 N/mm, respectively. Figure 7 shows the simulated annealing results of the optimized pulley radius of the underactuated anthropomorphic hand obtained as per Step 1, Fig 4. Flowchart of optimization. Figure 8 shows the results of the optimized spring pre-load angles of the

https://doi.org/10.1017/S0263574722000753 Published online by Cambridge University Press

Table III. *Optimized parameters of the underactuated anthropomorphic hand through PGR.*

Parameter	r_{tmcp}	r_{tpip}	r_{tdip}	r_{imcp}	r_{ipip}	r_{idip}	r_{mmcp}	r_{mpip}	r_{mdip}	r_{rmcp}	r_{rpip}	r_{rdip}	r_{lmcp}	r_{lpip}	r_{ldip}
Value (mm)	5	7	9	5	9	8	9	7	9	5	5	5	5	5	9
Parameter	θ_{tmcp}	θ_{tpip}	θ_{tdip}	θ_{imcp}	θ_{ipip}	θ_{idip}	θ_{mmcp}	θ_{mpip}	θ_{mdip}	θ_{rmcp}	θ_{rpip}	θ_{rdip}	θ_{lmcp}	θ_{lpip}	θ_{ldip}
Value (rad)	0.1	0.08	0.4	0.25	0.20	0.11	0.06	0.01	0.58	0.00	0.02	0.36	0.00	0.32	0.07

Table IV. *Optimized parameters of the underactuated anthropomorphic hand through unbalanced torque method.*

Parameter	r_{tmcp}	r_{tpip}	r_{tdip}	r_{imcp}	r_{ipip}	r_{idip}	r_{mmcp}	r_{mpip}	r_{mdip}	r_{rmcp}	r_{rpip}	r_{rdip}	r_{lmcp}	r_{lpip}	r_{ldip}
Value (mm)	7	7	7	9	7	9	6	9	7	6	7	8	9	7	8
Parameter	θ_{tmcp}	θ_{tpip}	θ_{tdip}	θ_{imcp}	θ_{ipip}	θ_{idip}	θ_{mmcp}	θ_{mpip}	θ_{mdip}	θ_{rmcp}	θ_{rpip}	θ_{rdip}	θ_{lmcp}	θ_{lpip}	θ_{ldip}
Value (rad)	0.01	0.00	0.40	0.23	0.13	0.40	0.38	0.08	0.78	0.00	0.00	0.00	0.06	0.00	0.31

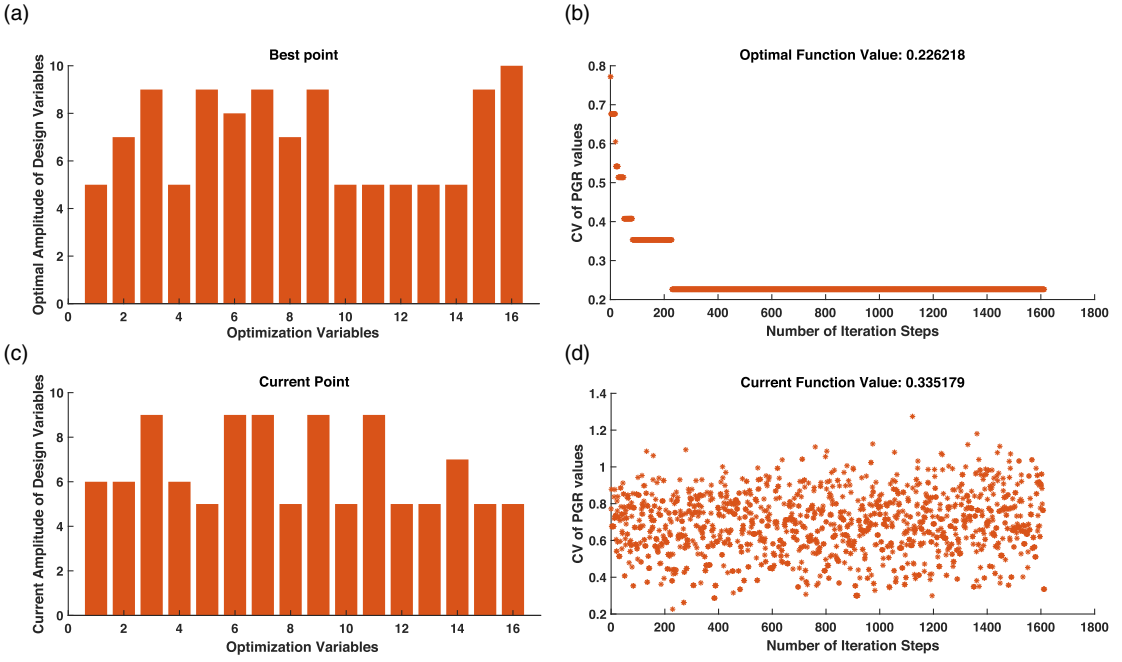

Figure 7. *Optimization plot of the various pareto-dominant solutions of pulley radius, Refer Table 3, Row 1 (Optimization performed as per Step 1, Fig 4: Flowchart of the optimization): (a) Magnitudes of Optimal Design Variable (1–15: Pulley Radius (units: mm), 16: Spring Stiffness (units: N/m, values: multiplied by 10)) (b) Optimal values of CV of PGRs (c) Magnitudes of Current Design Variable (1–15: Pulley Radius (units: mm), 16: Spring Stiffness (units: N/m, values: multiplied by 10)) (d) Current values of CV of PGRs.*

underactuated anthropomorphic hand obtained as per Step 2, Fig 4. Flowchart of optimization. The evolutionary algorithm results show the Pareto optimality or Pareto efficiency of the candidate optimal solutions, as no other change in the magnitude of design variables leads to improved optimal function value.

https://doi.org/10.1017/S0263574722000753 Published online by Cambridge University Press

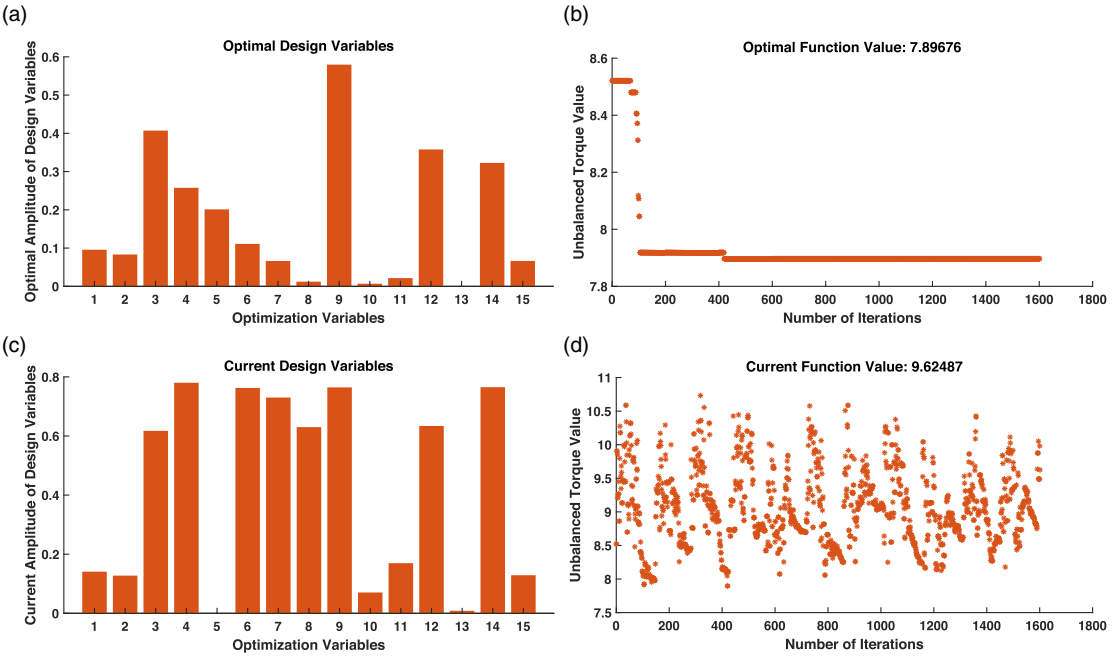

Figure 8. *Optimization plot of the various pareto-dominant solutions of Spring Pre-Load Angles, Refer Table 3, Row 2 (Optimization performed as per Step 2, Fig 4: Flowchart of the optimization): (a) Magnitudes of Optimal Design Variable (b) Optimal Unbalanced Torque Value (c) Magnitudes of Current Design Variable (d) Current Unbalanced Torque Value.*

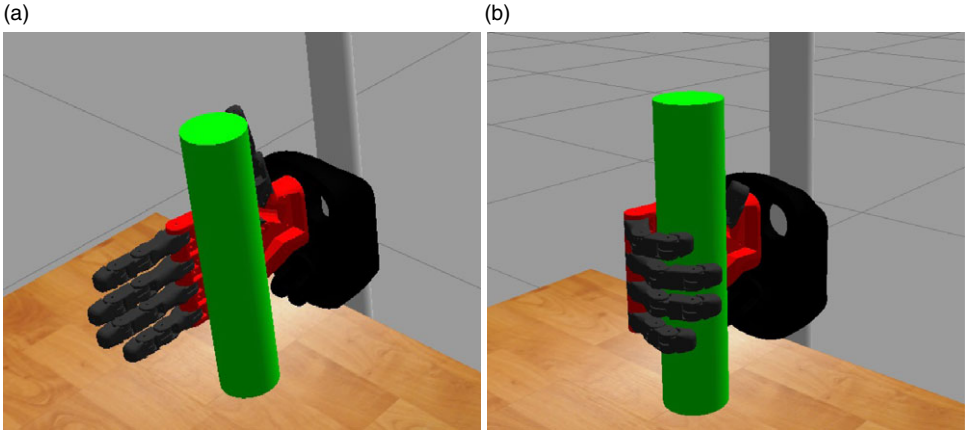

Figure 9. *Simulated anthropomorphic hand in gazebo simulation engine.*

6.2. Validation: Grasp quality based on GWS

For validation of the results obtained, we provided a physics engine-based simulation of the hand grasping an object in the ROS-Gazebo environment. The gazebo world environment is shown in Fig. 9(a). To simulate the actuation through the tendons, we enforce underactuation by coupling joint torques $\boldsymbol{\tau} \in \mathbb{R}^{3d}$, where d is the number of fingers of the hand, according to

$$\tau = Rf_t - Kq - \boldsymbol{\tau}_d \dot{q} \tag{19}$$

https://doi.org/10.1017/S0263574722000753 Published online by Cambridge University Press

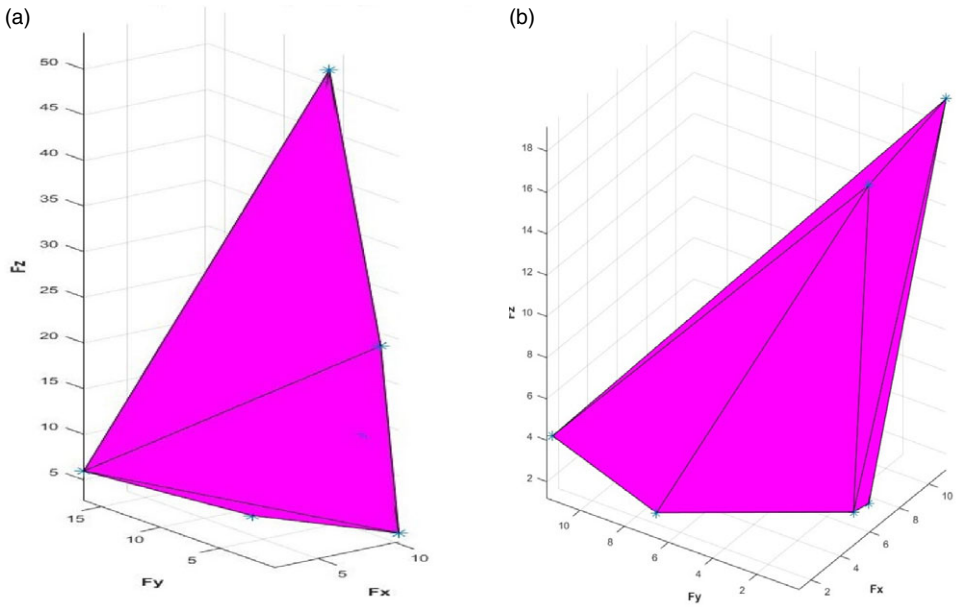

GWS of PGR optimized, $Q_\epsilon = 10.15$

GWS of unbalanced torque optimized, $Q_\epsilon = 4.49$

Figure 10. *Grasp Wrench Space showing the convex hull computed over the primitive wrench space. The grasp quality metric, $Q_\in$ and the number of wrench vectors, n are also shown.*

where R is a $3d \times d$ matrix determining the distribution of the tendon forces on the joints. Matrix K is a $3d \times 3d$ diagonal stiffness matrix where its values are defined by the coefficients of the springs mounted on each joint. Vectors $q \in R^{3d}$ and $\dot{q} \in R^{3d}$ are the joint angles and angular velocities, respectively, measured within the simulator. $\tau_d(\dot{q})$ is the damping vector and can also include torsional friction at the joints. In this formulation, the d input values are the actuator's angles ϕ, and they determine the $3d$ finger joint torques and, by that, simulate underactuation. For the same dynamics, we gave the same amount of effort to the actuator for both the optimized hands. Contact sensors were embedded onto the links of the fingers. The embedded sensors helped us to generate the grasp wrench data and subsequently, the wrench measures were received. The final grasp configuration is shown in Fig. 9(b).

GWS of the grasped forces for the two different underactuated hand designs, obtained through optimization by both the grasp quality metric and unbalanced torque methodology, was used for comparison. Considering a set of primitive wrenches, $\boldsymbol{\psi}$ obtained from the contact sensors embedded at the fingers, we get the GWS as

$$GWS = CH(\boldsymbol{\psi}) \tag{20}$$

where, GWS is the convex hull (CH) of the primitive wrenches, $\boldsymbol{\psi}$ [9]. The grasp quality measure is then computed as the radius of the largest ball inscribed inside the convex hull of GWS, which is referred to as the largest-minimum resisted wrench ($Q_\in$).

$$Q_\in = \min_{\boldsymbol{\psi} \in GWS} \|\boldsymbol{\psi}\| \tag{21}$$

The convex hull of the GWS obtained through the PGR optimization and the unbalanced torque method are shown in Fig. 10(a) and (b) respectively. The $Q_\in$ measure came out to be 10.15 for the PGR optimized hand and 4.49 for the unbalanced torque optimized hand. The Q_ϵ measure provides the magnitude of the largest perturbation wrench that the grasp can resist in any direction. Hence, the more the value of Q_ϵ, the more external wrench the grasp can resist with limited contact forces over all wrench directions. Due to its direct relation with the wrench domain, its result can be used to verify

https://doi.org/10.1017/S0263574722000753 Published online by Cambridge University Press

and cross-check various grasping tasks [17]. The results show the promise of better grasp quality for the underactuated hand-optimized through grasp quality metric.

7. Conclusion

This paper optimized the design parameters viz. pulley radii, pre-load angles and spring stiffness for an underactuated hand. Soft synergistic compliant grasping model was exploited to generate the different human grasps. We utilized the PGR measure as the objective function for optimization of the underactuated parameters. Further, validation of the results was performed on a ROS-Gazebo environment. The optimization method seems to be encouraging, as evident from the results of GWS analysis. As a next step, other grasp types and quality measures can be taken into account for comparative analysis. Further, lower level grasp control, like slippage and deformation prevention, can be embedded into the optimization objective function, so that the optimization framework can automatically take into account the manipulation behavior in the design stage.

Acknowledgements. The authors would like to acknowledge the help received from Maria Pozzi of University of Siena, Department of Information Engineering and Mathematics, Siena, Italy with the codes related to PGR.

Author contributions. Hirakjyoti Basumatary and Shyamanta M. Hazarika conceived and designed the work. Hirakjyoti Basumatary performed the simulations and generation of results. Shyamanta M. Hazarika guided the progress and reviewed the work.

Financial support. This work was supported in part by MHRD, Government of India through Indian Institute of Technology, Guwahati for Doctoral Research. Financial support received from DST, Government of India under Project Grant TDP/BDTD/21/2019 is gratefully acknowledged.

Conflicts of interest. None.

Ethical considerations. None.

References

[1] E. Noce, A. D. Bellingegni, A. L. Ciancio, R. Sacchetti, A. Davalli, E. Guglielmelli and L. Zollo, "Emg and eng-envelope pattern recognition for prosthetic hand control," *J. Neurosci. Meth.* **311**(1), 38–46 (2019).
[2] A. M. Votta, S. Y. Günay, B. Zylich, E. Skorina, R. Rameshwar, D. Erdogmus and C. D. Onal, *Kinematic Optimization of An Underactuated Anthropomorphic Prosthetic Hand* (2020) pp. 3397–3403.
[3] H. Basumatary and S. M. Hazarika, "State of the art in bionic hands," *IEEE Trans. Hum.-Mach. Syst.* **50**(2), 116–130 (2020).
[4] Z. Xu, "The Functional Capacity of the Humanlike Robotic Hands," **In:** *Hand Function* (Springer, 2019) pp. 291–312.
[5] R. Balasubramanian and A. M. Dollar, "Performance of Serial Underactuated Mechanisms: Number of Degrees of Freedom and Actuators," **In:** *Redundancy in Robot Manipulators and Multi-Robot Systems* (Springer, 2013) pp. 1–13.
[6] R.Xu and Ü. Özgüner, "Sliding mode control of a class of underactuated systems," *Automatica* **44**(1), 233–241 (2008).
[7] K. Xu, H. Liu, Y. Du and X. Zhu, "Design of an underactuated anthropomorphic hand with mechanically implemented postural synergies," *Adv. Robot.* **28**(21), 1459–1474 (2014).
[8] N. M. Kakoty, A Biomimetic Hand with EMG Based Grasp Emulation, PhD Thesis, Computer Sc. & Engg., Tezpur University (2014)
[9] M. A. Roa and R. Suárez, "Grasp quality measures: review and performance," *Auton. Robot.* **38**(1), 65–88 (2015).
[10] L. Wen, Y. Li, M. Cong, H. Lang and Y. Du, "Design and Optimization of A Tendon-Driven Robotic Hand," **In:** *2017 IEEE International Conference on Industrial Technology (ICIT)*(IEEE, 2017) pp. 767–772.
[11] R. Datta, S. Pradhan and B. Bhattacharya, "Analysis and design optimization of a robotic gripper using multiobjective genetic algorithm," *IEEE Trans. Syst. Man Cybern. Syst.* **46**(1), 16–26 (2015).
[12] H. Dong, E. Asadi, C. Qiu, J. Dai and I.-M. Chen, "Geometric design optimization of an under-actuated tendon-driven robotic gripper," *Robot. Comput.-Integr. Manuf.* **50**, 80–89 (2018).
[13] H. D. Salman, S. H. Bakhy and M. N. Hamzah, "Design and Optimization of Coupled and Self-Adaptive of an Underactuated Robotic Hand Using Particle Swarm Optimization," **In:** *IOP Conference Series: Materials Science and Engineering, vol. 928* (IOP Publishing, 2020) p. 022153.
[14] T. Ko, "A tendon-driven robot gripper with passively switchable underactuated surface and its physics simulation based parameter optimization," *IEEE Robot. Automat. Lett.* **5**(4), 5002–5009 (2020).

https://doi.org/10.1017/S0263574722000753 Published online by Cambridge University Press

[15] W. S. You, Y. H. Lee, G. Kang, H. S. Oh, J. K. Seo and H. R. Choi, "Kinematic design optimization for anthropomorphic robot hand based on interactivity of fingers,"*Intel. Serv. Robot.* **12**(2), 197–208 (2019).
[16] T. Chen, L. Wang, M. Haas-Heger and M. Ciocarlie, "Underactuation design for tendon-driven hands via optimization of mechanically realizable manifolds in posture and torque spaces," *IEEE Trans. Robot.* **36**(3), 708–723 (2020).
[17] M. Pozzi, M. Malvezzi and D. Prattichizzo, "On grasp quality measures: Grasp robustness and contact force distribution in underactuated and compliant robotic hands," *IEEE Robot. Automat. Lett*. **2**(1), 329–336 (2016).
[18] D. Prattichizzo, J. K. Salisbury and A. Bicchi, "Contact and Grasp Robustness Measures: Analysis and Experiments," **In:** *Experimental Robotics IV* (Springer, 1997) pp. 83–90.
[19] M. Malvezzi and D. Prattichizzo, "Evaluation of Grasp Stiffness in Underactuated Compliant Hands," **In:** *2013 IEEE International Conference on Robotics and Automation*(IEEE, 2013) pp. 2074–2079.
[20] D. Prattichizzo and J. C. Trinkle, "Grasping," **In:** *Springer Handbook of Robotics* (Springer, 2016) pp. 955–988.
[21] E. Farnioli, M. Gabiccini and A. Bicchi, "Quasi-Static Analysis of Synergistically Underactuated Robotic Hands in Grasping and Manipulation Tasks," **In:** *Human and Robot Hands* (Springer, 2016) pp. 211–233.
[22] M. Malvezzi, G. Salvietti and D. Prattichizzo, "Evaluation of Grasp Stiffness in Underactuated Compliant Hands Exploiting Environment Constraints," **In:** *ROMANSY 22–Robot Design, Dynamics and Control* (Springer, 2019) pp. 409–416.
[23] L. Almeida and P. Moreno, "Potential Grasp Robustness for Underactuated Hands: New Heuristics and Uncertainty Considerations," **In:** *2020 IEEE International Conference on Autonomous Robot Systems and Competitions (ICARSC)* (IEEE, 2020) pp. 233–238.
[24] A. Bicchi, "On the closure properties of robotic grasping," *Int. J. Robot. Res*. **14**(4), 319–334 (1995).
[25] M. Malvezzi, G. Gioioso, G. Salvietti and D. Prattichizzo, "Syngrasp: A matlab toolbox for underactuated and compliant hands," *IEEE Robot. Autom. Mag.* **22**(4), 52–68 (2015).
[26] A. Bicchi, "Force Distribution in Multiple Whole-Limb Manipulation," **In:** *[1993] Proceedings IEEE International Conference on Robotics and Automation* (IEEE, 1993) pp. 196–201.
[27] C. I. Mavrogiannis, C. P. Bechlioulis, M. V. Liarokapis and K. J. Kyriakopoulos, "Task-specific Grasp Selection for Underactuated Hands," **In:** *2014 IEEE International Conference on Robotics and Automation (ICRA)* (IEEE, 2014) pp. 3676–3681.

Appendix

A. Compliant grasp model

The classical grasp model assumes rigid bodies, point contacts, and is quasistatic, that is, inertial forces are ignored. However, for more realistic modeling, the rigid body model can be extended to include compliance. Introducing compliance in the grasp model helps implement compliant behavior of the hand and the grasped object thus, increasing the contact area and thereby the robustness of the grasp. Details of the compliant grasp model are given in the next section. The nomenclatures describing the mathematical symbols have been included in the Table I.

A.1. The complaint grasp model

In static equilibrium conditions, by utilizing the virtual work principle, we can write the equation of object and hand equilibrium, respectively as 19:

$$\boldsymbol{w} = -G\boldsymbol{\lambda} \tag{1}$$

$$\boldsymbol{\tau} = J^T\boldsymbol{\lambda} \tag{2}$$

However, if $\mathcal{N}(G) \cap \mathcal{N}(J^T) \neq 0$, then the solution of the two algebraic system of equations, that is, Eq. (1) is not unique. Bicchi et al. [26] solved this problem by framing the problem into a linearized quasistatic system. The method extends the rigid-body model to include compliance and assumes that the contact constraint violation and contact force variation are related through a contact stiffness model. This problem usually occurs in a power grasp for an underactuated hand, when the number of contacts points is more than the controllable degrees of freedom.

In modeling the compliant underactuated grasp, a set of hypothetical springs are introduced at the contact locations between the object and the fingers. The contact force variation $\delta\boldsymbol{\lambda}$ from the initial equilibrium position is given as:

$$\delta\boldsymbol{\lambda} = K_c(\delta\boldsymbol{c}^h - \delta\boldsymbol{c}^o) = K_c(\mathbf{J}\delta\boldsymbol{q} - \mathbf{G}^T\delta\boldsymbol{u}) \tag{3}$$

https://doi.org/10.1017/S0263574722000753 Published online by Cambridge University Press

The actual joint variables, $\boldsymbol{q}$, may differ from the reference one, $\boldsymbol{q_r}$, if the hand structural parameters are not perfectly stiff. This can be modeled as:

$$\delta\boldsymbol{\tau} = K_q(\delta\boldsymbol{q_r} - \delta\boldsymbol{q}) \tag{4}$$

The hand joint reference configuration $\boldsymbol{q_r}$ for an underactuated hand is defined with lower-dimensional inputs than the number of DoF (hand joints), that is, we consider that the relative movements of the joints are coupled/constrained. A vector z, named Lagrangian variables, is introduced, whose dimensionality equals the number of DoFs of the hand.

The Lagrangian variables can be split up as $z = \left[z_a^T \;\; z_p{}^T\right]^T$, with dimension $n_z = n_{za} + n_{zp}$ with $\boldsymbol{z_a}$ representing the active/controllable input variables (e.g., actuators) while the variables, $\boldsymbol{z_p}$, representing the passive/uncontrollable variables (e.g., the spring system).

The joint references $\boldsymbol{q_r}$, as a function of the Lagrangian variables z, is defined as:

$$\boldsymbol{q_r} = f_z(z) \tag{5}$$

where, $f_z : \mathbb{R}^{n_z} \rightarrow \mathbb{R}^{n_q}$ represents non–linear kinematic relationship. We can express the above equation in a linearized form, by introducing a coupling matrix called synergy matrix, S [19], and express the variation of joint reference variable as a function of Langrangian variable variation.

$$\delta\boldsymbol{q_r} = S\delta z \tag{6}$$

The postural synergy based underactuation is imposed upon the grasping system by means of the synergy matrix.

The external contact wrenches can be expressed in the Lagrangian co-ordinate as

$$\boldsymbol{\sigma} = S^T\boldsymbol{\tau} \tag{7}$$

$\boldsymbol{\sigma}$ can be splitted as

$$\boldsymbol{\sigma_a} = S_a{}^T\boldsymbol{\tau} \qquad \boldsymbol{\sigma_p} = S_p{}^T\boldsymbol{\tau} \tag{8}$$

The above equation represents the contribution to hand equilibrium of the forces generated by the actuators, $\boldsymbol{\sigma_a}$ (active Lagrangian forces) and of the passive elements, $\boldsymbol{\sigma_p}$ (passive Lagrangian forces).

A.2. Soft synergies

The postural synergy-based kinematic model is insufficient to explain a grasp by an underactuated multi-fingered hand accurately. In addition, the interaction with a grasped object must be represented and included in the study. This has recently been accomplished using "Soft Synergy," a modeling framework that allows synergies to control the hand's kinematics in such a way that the final posture matches the geometry of the gripped object. This is accomplished by taking into account the hand's structural compliance as well as the object's rigidity. Specifically, during a grip, forces appear as the fingers of the hand make contact with the object, and torques appear at the finger joints as a result of these forces. These torques alter hand posture based on contact and joint compliance, allowing the hand to conform to the shape of the object [27].

In the Lagrangian co-ordinate space, assuming close loop control of the position of actuators, the actuation forces are expressed as

$$\delta\boldsymbol{\sigma_a} = K_{za}(\delta\boldsymbol{z_{ra}} - \delta\boldsymbol{z_a}) \tag{9}$$

$$\delta\boldsymbol{\sigma_p} = -K_{zp}\delta\boldsymbol{z_p} \tag{10}$$

Hence, we can write

$$\delta\boldsymbol{\sigma} = \begin{bmatrix}\delta\boldsymbol{\sigma_a}\\ \delta\boldsymbol{\sigma_p}\end{bmatrix} = K_z(\delta\boldsymbol{z_r} - \delta z) \tag{11}$$

https://doi.org/10.1017/S0263574722000753 Published online by Cambridge University Press

$$K_z = \begin{bmatrix} K_{za} & 0 \\ 0 & K_{zp} \end{bmatrix}, \quad \delta z_r = \begin{bmatrix} \delta z_{ra} \\ 0 \end{bmatrix}, \quad \delta z = \begin{bmatrix} \delta z_a \\ \delta z_p \end{bmatrix} \tag{12}$$

A.3. Compliant grasp analysis in underactuated hands

The linearization of object equilibrium of Eq. (1), yields the following expression in quasi-static condition

$$\delta \boldsymbol{w} + G\delta \boldsymbol{\lambda} = 0 \tag{13}$$

Further, the linearization of the hand equilibrium of Eq. (2), yields the joint torque variation expression as

$$\delta \boldsymbol{\tau} = J^T \delta \lambda + K_{J,q}\delta \boldsymbol{q} + K_{J,u}\delta \boldsymbol{u} \tag{14}$$

where, $K_{J,q}\delta \boldsymbol{q} = \frac{\partial J^T \boldsymbol{\lambda}_0}{\partial \boldsymbol{q}}$ and $K_{J,u}\delta \boldsymbol{q} = \frac{\partial J^T \boldsymbol{\lambda_0}}{\partial \boldsymbol{u}}$, that is, the derivatives of hand Jacobian matrix wrt $\boldsymbol{q}$ and $\boldsymbol{u}$.

Variation of the Lagrangian forces can be expressed as

$$\delta \boldsymbol{\sigma} = S^T \delta \boldsymbol{\tau} + K_{S,z}\delta z \tag{15}$$

where, $K_{S,z} = \frac{\partial S^T \boldsymbol{\tau_0}}{\partial \boldsymbol{z}}$. Here, since S is constant, therefore $K_{S,z} = \mathbf{[0]}$ [19].

All the main Eqs. (4), (6), (11), (13), (14), (15) can be summarized in the equation:

$$A\delta \boldsymbol{x} = \delta \boldsymbol{y} \tag{16}$$

$$A = \begin{bmatrix} -G & 0 & 0 & 0 & 0 & 0 & 0 \\ J^T & K_{J,u} & -I & K_{J,q} & 0 & 0 & 0 \\ 0 & 0 & S^T & 0 & -I & K_{S,z} & 0 \\ C_c & G^T & 0 & -J & 0 & 0 & 0 \\ 0 & 0 & -I & -K_q & 0 & 0 & K_q \\ 0 & 0 & 0 & 0 & C_z & I & 0 \\ 0 & 0 & 0 & 0 & 0 & S & -I \end{bmatrix} \tag{17}$$

$$\delta \boldsymbol{x} = \begin{bmatrix} \delta \boldsymbol{\lambda} & \delta \boldsymbol{u} & \delta \boldsymbol{\tau} & \delta \boldsymbol{q} & \delta \boldsymbol{\sigma} & \delta z & \delta \boldsymbol{q_r} \end{bmatrix}^T \tag{18}$$

$$\delta \boldsymbol{y} = [\delta \boldsymbol{w} \;\; 0 \;\; 0 \;\; 0 \;\; 0 \;\; \delta z_r \;\; 0]^T \tag{19}$$

B. Grasp quality metric: Potential grasp robustness (PGR)

Applying perturbations to initial equilibrium configuration produces new contact force distribution expressed as $\boldsymbol{\lambda} = \boldsymbol{\lambda_0} + \delta \boldsymbol{\lambda}$. Considering i-th contact, the contact forces $\boldsymbol{\lambda}_i$ requires to satisfy unilateral constraint and Coulomb friction constraint in Eqs. (20) and (21) respectively. These constraints helps in avoiding slip and detachment of the contact during object grasps.

$$\boldsymbol{\lambda}_{i,n} \geq 0 \tag{20}$$

$$\sqrt{\boldsymbol{\lambda}_{i,t}^2 + \boldsymbol{\lambda}_{i,o}^2} \leq \mu_i \boldsymbol{\lambda}_{i,n} \tag{21}$$

Let us consider, $\boldsymbol{d}\,(\boldsymbol{\lambda}) = \left[\boldsymbol{d}_{1,c}, \boldsymbol{d}_{1,f}, \boldsymbol{d}_{1,\max} \ldots .., \boldsymbol{d}_{n_c,c}, \boldsymbol{d}_{n_c f}, \boldsymbol{d}_{n_c,\max}\right]$ where $\boldsymbol{d}_{1,c}$ represents contact force in the normal direction, $\boldsymbol{d}_{1,f}$, distance of $\boldsymbol{\lambda}_i$ from the friction cone surface and $\boldsymbol{d}_{i,\max} = f_{i,\max} - \|\boldsymbol{\lambda}_i\|$, maximum force $f_{i,max}$ applied at the individual contact points.

https://doi.org/10.1017/S0263574722000753 Published online by Cambridge University Press

In $\mathbb{R}^{3n}$, the inequality $\|\delta\boldsymbol{\lambda}\| \leq \|\boldsymbol{d}(\boldsymbol{\lambda})\|_\infty$ expresses a sphere which is centered inside the equilibrium contact force. In order to prevent slip, the preceding inequality is a sufficient condition on the maximum euclidean norm of perturbations of the contact forces $\delta\boldsymbol{\lambda}$ in order to prevent slip at the contact points. This property is referred to as "contact robustness".

The limiting space of $\boldsymbol{d}(\boldsymbol{\lambda})$, described in the contact wrench space, must be mirrored in the space of external disturbances $\delta\boldsymbol{w}$ acting on the grasped object, to evaluate its contact robustness.

In the quasi-static condition, the grasping contact forces and the grasped object disturbance wrenches can be written as:

$$\delta\boldsymbol{\lambda} = -G_K^R \delta\boldsymbol{w} \tag{22}$$

The ellipsoid in the wrench space centered in zero and with major principal axes of length $2\|\boldsymbol{d}\|_\infty / \boldsymbol{\sigma_k}(G_K^R)$, is described by the relationship $\delta\boldsymbol{\lambda}^T\delta\boldsymbol{\lambda} = \delta\boldsymbol{w}^T {G_K^R}^T G_K^R \delta\boldsymbol{w} \leq \|d\boldsymbol{\lambda}\|_\infty^2$, which is derived from the preceding equation, Eq. (22). Despite the wrench disturbance, the inscribed sphere with radius, $\dfrac{\|\boldsymbol{d}(\lambda)\|}{\boldsymbol{\sigma_{max}}(G_K^R)}$, constitutes a restriction on the euclidean norm of $\delta\boldsymbol{w}$ ensuring that all contact requirements hold. As a result, in quasistatic condition a particular grasp may withstand any disturbance wrench $\delta\boldsymbol{w}$ without defying the constraints given by Eqs. (20) and (21), that is, to say without separation and slippage at any contact point provided that

$$\|\delta\boldsymbol{w}\| \leq \frac{\|\boldsymbol{d}(\boldsymbol{\lambda})\|}{\boldsymbol{\sigma_{max}}(G_K^R)} \tag{23}$$

The internal forces which are controllable belongs to the subspace $\mathcal{F}_h$ [17]

$$\mathcal{F}_h = \mathcal{R}(E) = \mathcal{N}(G) \cap (\mathcal{R}(KJS) + \mathcal{R}(KG^T)) \tag{24}$$

where matrix $E \in \mathbb{R}^{n_\lambda \times h}$ represents a base of the subspace and $K = ({K_c}^{-1} + J{K_q}^{-1}J^T)^{-1}$. The controllable internal forces is expressed as $\delta\boldsymbol{\lambda_h} = E\boldsymbol{y}$, where $\boldsymbol{y} \in \mathbb{R}^h$, generic vector.

Considering $\boldsymbol{d}_{\min}^{\mathcal{F}_h}$ is the minimum of the vector $\boldsymbol{d}(\boldsymbol{\lambda})$, which is calculated using controllable contact forces $\boldsymbol{\lambda} = G_K^R\boldsymbol{w} + E\boldsymbol{y}$, where $G_K^R = KG^T(GKG^T)^{-1}$. Sufficient condition for the maximum force constraint and friction constraints to be satisfied even during a contact force perturbation $\delta\boldsymbol{\lambda}$ is given as : $\|\delta\boldsymbol{\lambda}\| \leq d_{\min}^{\mathcal{F}_h}$

Considering the external wrench distribution we get

$$\|\delta\boldsymbol{w}\| \leq \frac{\boldsymbol{d}_{\min}^{\mathcal{F}_h}}{\boldsymbol{\sigma_{max}}(G_K^R)} \tag{25}$$

where, $\boldsymbol{\sigma_{max}}$: maximum singular value

Since $\boldsymbol{d}_{\min}^{\mathcal{F}_h}$ depends on $\boldsymbol{y}$, optimal contact force distribution is given by $\hat{\boldsymbol{\lambda}}_{opt} = G_K^R\boldsymbol{g} + E\hat{\boldsymbol{y}}_{opt}$ where $\hat{\boldsymbol{y}}_{\boldsymbol{opt}} = \arg\max\,(\boldsymbol{d}_{\min}^{\mathcal{F}_h}/\boldsymbol{\sigma_{max}}(G_K^R))$ [17].

The grasp quality metric, PCR, which assumes friction constraints to be satisfied at all contact points is expressed as:

$$PCR = \max_{\boldsymbol{y}} \frac{\boldsymbol{d}_{\min}^{\mathcal{F}_h}}{\boldsymbol{\sigma_{max}}(G_K^R)} \tag{26}$$

On the other hand, grasp robustness metric called PGR (potential grasp robustness), shows that even if some contacts are lost a grasp can be stable

$$PGR = \max_{C_j} \max_{\boldsymbol{y}} \frac{\boldsymbol{d}_{\min}^{\mathcal{F}_h}(C_j)}{\boldsymbol{\sigma_{max}}(G_{K(C_j)}^R)} \tag{27}$$

$$subject\ \ to \quad \mathcal{N}(K(C_j)G^T) = 0 \tag{28}$$

where C_j are 3 contact states (j =1,2,3) as described below:

https://doi.org/10.1017/S0263574722000753 Published online by Cambridge University Press

- Contact State 1: Contact forces are exerted in all directions via the contact locations and therefore, $K_{ic} = diag(K_{itx}, K_{ity}, K_{itn})$, where K_{ic}: contact stiffness matrix; K_{itx} and K_{ity}: tangential stiffnesses; K_{itn}: normal stiffness.
- Contact State 2: Contact forces are exerted only in normal direction and $K_{ic} = K_{itn}$.
- Contact State 3: Contact is considered as detached and $K_{ic} = \mathbf{[0]}$.

Cite this article: H. Basumatary and S. M. Hazarika (2022). "Design optimization of an underactuated tendon-driven anthropomorphic hand based on grasp quality measures", Robotica **40**, 4056–4075. https://doi.org/10.1017/S0263574722000753